Commun. Comput. Phys.
doi: 10.4208/cicp.OA-2020-0028

Vol. **29**, No. 2, pp. 445-471
February 2021

On Accurately Resolving Detonation Dynamics by Adaptive Finite Volume Method on Unstructured Grids

Yana Di[1,2], Guanghui Hu[3,4,*], Ruo Li[5] and Feng Yang[5]

[1] *Institute of Mathematical Research, Beijing Normal University & UIC, Zhuhai, China.*
[2] *Programme of Applied Mathematics, BNU-HKBU United International College, Zhuhai, Guangdong Province, China.*
[3] *Department of Mathematics, Faculty of Science and Technology, University of Macau, Macao SAR, China.*
[4] *Zhuhai UM Science & Technology Research Institute, Zhuhai, Guangdong Province, China.*
[5] *CAPT, LMAM, and School of Mathematical Science, Peking University, Beijing, China.*

Received 10 February 2020; Accepted (in revised version) 1 June 2020

Abstract. Long time simulations are needed in the numerical study of the Zeldovich-Neumann-Döring model, in which the quality resolving the dynamics of the detonation front is crucial. The numerical error introduced from the inappropriate outflow boundary condition and the mesh resolution are two main factors qualitatively affecting the dynamics of the detonation front. In this paper we improve the numerical framework in [15] by introducing the Strang splitting method and a new *h*-adaptive method with a feature based *a posteriori* error estimator. Then a cheap numerical approach is proposed to sharply estimate a time period, in which the unphysical influence on the detonation front can be avoided effectively. The sufficiently dense mesh resolution can be guaranteed around the detonation front and in the reaction zone by the proposed *h*-adaptive method. The numerical results show that the proposed method is sufficiently robust even for long time calculations, and the quality dynamics of the detonation can be obtained by the proposed numerical approach.

AMS subject classifications: 65N50, 35Q31

Key words: Reactive Euler equations, Strang splitting scheme, *h*-adaptive methods, subsonic outflow boundary, ZND model.

*Corresponding author. *Email addresses:* yndi@uic.edu.cn (Y. Di), garyhu@umac.mo (G. Hu), rli@math.pku.edu.cn (R. Li), yangfengzzz@qq.com (F. Yang)

1 Introduction

The time-dependent, nonlinear reactive Euler equations have been playing an important role in the study of the detonation phenomenon. Since its intrinsic instability, in the high dimensional study of the detonation, there would be transverse fluctuation appearing along the detonation front, which can result in very complex dynamics in the following reaction zone. To well understand the mechanics of this unstable phenomenon would benefit the practical application of the detonation such as the design of the rotating detonation engine [23].

Although there have been many pioneer works [27,28] for the stability analysis on the detonation phenomenon, the linearization can not be avoided in most of them. It is the direct numerical simulation a method on fully resolving the nonlinearity of the governing equation, which has motivated the works such as [12, 13, 25, 35] for the finite difference methods, [4] for the finite volume methods, [7] for the finite element methods, [39] for the discontinuous Galerkin methods, etc. However, the advantages mentioned above from the direct numerical simulations can be obtained only if the simulations are quality, i.e., the dynamics of the detonation front is well resolved, and the simulation time is sufficiently long. Hence, it is demanding on the computational resource, especially for high dimensional simulations. To improve the efficiency of the implementation, several acceleration techniques have been applied on the numerical methods. For examples, the fractional time stepping methods in which the convection process and reaction process are treated as two independent processes. By combining these two processes with different orders, the numerical methods with different numerical accuracy with respect to the size of the time stepping can be obtained. We refer to [24] for the detail of the splitting methods, and [31] for the application of the splitting methods in the detonation simulations. The adaptive mesh methods also have been explored in depth on the simulations of the detonation phenomenon. The adaptive mesh methods optimize the distribution of the grid points according to some quantity such as the *a posteriori* error, so that the higher numerical accuracy can be obtained by using less grid points. This is an attractive technique for the detonation simulations since the solutions change dramatically only in a relatively small region, i.e., the detonation front and the following reaction zone, and the grid points of the mesh can be optimized by locating more points in those trouble regions. The author may refer to [5, 15, 34, 40] for the applications of the adaptive mesh methods in the detonation simulations. The author may also refer to [1, 9, 18, 30, 36, 37] for the successful applications of the adaptive mesh methods in other areas. Finally, with the development of the hardware, the parallel computing has been widely used to significantly accelerate the detonation simulations [29, 33].

Besides the efficiency, another issue on accurately resolving the dynamics of the detonation front is the outflow boundary conditions. In the ZND model, the detonation propagates in an infinitely long tube, with a constant velocity. To numerically study the wave propagation, a classical strategy is to introduce a moving frame with the same velocity, in which a stable detonation would be obtained, or the detonation front would

fluctuate around its initial position. In this case, a subsonic outflow boundary condition is needed in the simulation, which means that the pressure boundary condition can not be extrapolated from inside the domain, otherwise the numerical error would be introduced from the boundary, and this error would catch up with the detonation front in an sufficiently long time. Our numerical results show that, the detonation dynamics would be qualitatively affected if the error coincides with the unstable mode of the detonation. Consequently, it is an important issue to remove or restrain this kind of numerical error. Besides the non-reflecting boundary conditions [20, 26], to estimate the reliable period of the observation is another approach to get the reliable solutions. In [19, 22], for some cases, the upper bounds of the time duration for the reliable observation of the detonation dynamics are given, by the estimation of the propagation velocity of the error. However, based on our numerical experiments, it is found that those upper bounds are overestimated by using the aggressive estimation on the velocity, which unexpectedly causes a too long computational domain for a given time period of the observation. Consequently, it would also cause the non-ignorable increment on the CPU time since the extra amount of the mesh grids would be needed in the simulation. The situation is worse for higher dimensional problems.

In this paper, we propose a numerical approach to deliver a sharp estimation on the upper bound for time period of the reliable observation for the one-dimensional ZND models, and further demonstrate that such upper bound can be used in the high-dimensional problems with the same configuration of the model. It is noted that the cheap and reliable estimation from one-dimensional problem would result in the considerable saving on the computational resource in the high-dimensional simulations. The numerical framework in this paper for the two-dimensional reactive Euler equations is designed following the one in [15], in which the finite volume method is employed for the spatial discretization of the governing equation, while a second order Runge-Kutta method is adopted for the temporal discretization. The adaptive mesh method is used for improving the numerical accuracy and enhancing the implementation efficiency. And the algorithm is parallelized by OpenMP for the acceleration of the simulations. It is worth to mentioning that to improve the numerical framework in [15], the Strang splitting method is used to decouple the convection process and the reaction process, which prevent the time step constrained by the stiff source term. Moreover, with Strang splitting, the challenge on solving generalized Riemann problem can be avoided. It is noted that by using Strang splitting, because of stiff source term, even a stable numerical scheme may lead to spurious unphysical solutions unless the small chemical time scale is fully resolved numerically [2, 11]. In the h-adaptive method proposed in this paper, an error indicator, consisting of the information from the pressure and the reaction rate, is designed to conduct the local refinement of the mesh grids. The numerical results show that both the region of the detonation front and the reaction zone are partitioned with sufficiently many grid points, which benefit the implementation of the splitting method well.

The rest of the paper is organized as follows. In the next section, the reactive Euler equations, the numerical framework on solving the equations, as well as h-adaptive

methods are described in detail. In Section 3, the qualitative influence of the inappropriate outflow boundary condition on the dynamics of the detonation front is demonstrated by numerical examples, and a numerical approach is proposed for avoiding the issue. In Section 4, the effectiveness of the proposed numerical methods, as well as the performance of the *h*-adaptive methods, can be successfully observed from a number of numerical experiments. Finally, concluding remarks are given and a discussion of future work is outlined.

2 Numerical discretization

Although Chapman-Jouguet detonation theory works well on the prediction of the detonation speed, it gives no information on the internal solution structure in the reaction zone of the detonation since the assumption of infinitesimal region of the reaction zone. The theory is improved by Y. B. Zel'dovich [38], J. von Neumann [32], and W. Döring [6] by considering the finite chemical reaction rate, and the derived model is the well known ZND detonation model, which is still widely used in the detonation study nowadays. A brief introduction of the ZND theory can be found in Appendix A. It is noted that to facilitate the numerical study of the ZND models, a C++ program [8] is provided on GitHub for the generation of the one-dimensional ZND results, with given parameters.

In this section, we describe a numerical framework based on the finite volume method to solve the two-dimensional reactive Euler equations. The following is a brief summary of the proposed numerical method. First of all, we use Strang splitting strategy to separate the reaction process from the convection process of the fluid. Then a second order TVD Runge-Kutta scheme is used to solve ODEs derived from the splitting, while a second order Godunov type finite volume method is applied to solve the standard Euler equations.

2.1 Reactive Euler equations

At first, we need to resort to the following reactive Euler equations to study the multidimensional nature of the detonation,

$$\frac{\partial}{\partial t}\boldsymbol{U}+\nabla\cdot\boldsymbol{F}(\boldsymbol{U})=\boldsymbol{S}(\boldsymbol{U}), \tag{2.1}$$

where $\boldsymbol{U}$, $\boldsymbol{F}(\boldsymbol{U})$, and $\boldsymbol{S}(\boldsymbol{U})$ denote the conservative variable, flux, and source term, respectively. Their expressions are given as follows,

$$\boldsymbol{U}=\begin{bmatrix}\rho\\ \rho\boldsymbol{V}\\ E\\ \rho Y\end{bmatrix},\quad \boldsymbol{F}(\boldsymbol{U})=\begin{bmatrix}\rho\boldsymbol{V}\\ \rho\boldsymbol{V}\otimes\boldsymbol{V}+P\boldsymbol{I}\\ (E+P)\boldsymbol{V}\\ \rho Y\boldsymbol{V}\end{bmatrix},\quad \text{and}\quad \boldsymbol{S}(\boldsymbol{U})=\begin{bmatrix}0\\ 0\\ 0\\ \omega\end{bmatrix}, \tag{2.2}$$

where $\boldsymbol{V}=[u,v]^T$ denotes the velocity vector and $\otimes$ present the tensor product of velocity field. We use the following equation to close the above system,

$$E=P/(\gamma-1)+\rho\|\boldsymbol{V}\|^2/2+\rho YQ, \tag{2.3}$$

where ρ, $\boldsymbol{V}$, P, E, and Y stand for the density of the mixture, velocity, pressure, total energy, and the mass fraction of the reactant, respectively. And γ is the ratio of the specific heat, and Q is the amount of heat released per unit mass in the reaction. Based on the above assumption on the reaction, we define the reaction rate ω by

$$\omega=-k\rho Y, \tag{2.4}$$

where k is given by the Arrhenius law

$$k=Ae^{-E_a/T}. \tag{2.5}$$

Here A is the preexponential factor, E_a is the activation energy, and $T=P/\rho$ is the temperature.

It is noted that for the x-split Euler equations in two dimension, in which the conserved quantities and fluxes are given by

$$\boldsymbol{U}=\begin{bmatrix}\rho\\ \rho u\\ \rho v\\ E\\ \rho Y\end{bmatrix},\quad \boldsymbol{F}(\boldsymbol{U})=\begin{bmatrix}\rho u\\ \rho u^2+P\\ \rho uv\\ (E+P)u\\ \rho Yu\end{bmatrix}, \tag{2.6}$$

there are five eigenvalues, i.e., $u-c$, u (of multiplicity 3), and $u+c$. Here, the $c=\sqrt{\gamma\frac{P}{\rho}}$ is the speed of sound. The numerical methods in this paper are designed for solving the equations on the unstructured grids, which means that the numerical flux is imposed along the normal direction to the edge of a given triangle element. Although the equations will be different from above x-split form, the results are still applicable.

2.2 Strang splitting

Since its good balance between the numerical accuracy and the computational complexity, the second order Strang splitting strategy is always a competitive choice among the splitting methods. We refer to [24] for a recent review of the splitting methods.

The application of Strang splitting on solving (2.1) is described as follows. First, suppose that the solution at the time t_n is denoted by $\boldsymbol{U}_n$. What we want is the solution at the time t_{n+1}, i.e., $\boldsymbol{U}_{n+1}$. Let $\Delta t=t_{n+1}-t_n$ be the step size of the time. In Strang splitting, the convection-reaction process is split into three independent processes below.

S1: (*Reaction process*) By solving the following ODE, we get $\tilde{U}$.

$$\begin{cases} \dfrac{\partial}{\partial t}\tilde{\boldsymbol{U}} = \boldsymbol{S}(\tilde{\boldsymbol{U}}), \quad \text{on } (0,\Delta t/2], \\ \tilde{\boldsymbol{U}}(0) = \boldsymbol{U}_n. \end{cases} \tag{2.7}$$

S2: (*Convection process*) With the initial condition $\tilde{U}$, we get $\tilde{\tilde{U}}$ by solving the following Euler equations.

$$\begin{cases} \dfrac{\partial \tilde{\tilde{\boldsymbol{U}}}}{\partial t} + \nabla \cdot \boldsymbol{F}(\tilde{\tilde{\boldsymbol{U}}}) = 0, \quad \text{on } (0,\Delta t], \\ \tilde{\tilde{\boldsymbol{U}}}(0) = \tilde{\boldsymbol{U}}. \end{cases} \tag{2.8}$$

S3: (*Reaction process*) With the initial condition $\tilde{\tilde{U}}$, we finally get U_{n+1} by solving the following ODE

$$\begin{cases} \dfrac{\partial}{\partial t}\boldsymbol{U}_{n+1} = \boldsymbol{S}(\boldsymbol{U}_{n+1}), \quad \text{on } (0,\Delta t/2], \\ \boldsymbol{U}_{n+1}(0) = \tilde{\tilde{\boldsymbol{U}}}. \end{cases} \tag{2.9}$$

Remark 2.1. The numerical error introduced by the above Strang splitting is of $\mathcal{O}(\Delta t^2)$. There are extensions of the splitting schemes for the higher order [24]. However, it can not be avoided to introduce the negative coefficients in the scheme, which may cause the stability issue.

Remark 2.2. If we combine the last reaction process of the current propagation step to the first reaction process of the next propagation step, Strang splitting will have no difference to the first order splitting scheme, except for the first and the last propagation steps. This can be used to accelerate the simulations.

In the following subsections, we give detailed discussion on the numerical methods for the reaction process and the convection process, respectively.

2.3 Second order Runge-Kutta scheme for reaction process

To balance the stability and the numerical accuracy, the second order Runge-Kutta scheme is used to solve the ODEs in the reaction process as follows.

$$\begin{cases} \boldsymbol{U}^{\frac{1}{2}} = \boldsymbol{U}^{(m)} + \dfrac{1}{2}\tilde{\Delta} t \boldsymbol{S}(\boldsymbol{U}^{(m)}), \\ \boldsymbol{U}^{(m+1)} = \boldsymbol{U}^{(m)} + \tilde{\Delta} t \boldsymbol{S}(\boldsymbol{U}^{\frac{1}{2}}), \end{cases} \tag{2.10}$$

where $\tilde{\Delta} t$ is the sub-time step size for the partition in $[0,\Delta t/2]$. For the partition with M subintervals, we have $\Delta t = 2M\tilde{\Delta} t$, and $U^{(m)}$ represents the conserved quantity at the sub-time $m\tilde{\Delta} t$ for $m = 0,1,2,\cdots,M-1$.

In the general cases, the time scale of for the reaction process is several orders of magnitude faster than that for the convection process, which introduces very severe numerical stiffness in the simulations [14]. There are many excellent methods in the market to resolve this stiffness problem, such as the random projection method in [2]. In our work, we solve the above ODEs directly with the sufficiently small time steps. Several acceleration techniques are proposed to enhance the efficiency, based on the following observation.

It is noted that although the amount of ODEs is equal to the number of the elements in the mesh, which could be dramatically large especially in the high dimensional problems, each ODE is solved completely independently. This is a perfect scene for the use of parallelization. The only issue is the possibly bad balancing of the work load in the case that considerably many ODEs from the reaction zone are assigned to one single processing. In our work, the OpenMP parallelization is used to handle those ODEs. To resolve the possible bad balancing of the work load, the computational domain is split into a number of subdomains, in which each single subdomain occupies equal part of the reaction zone. This can be done trivially for the problems in this paper. However, for the general cases, the partition of the subdomains needs to be designed carefully.

2.4 Second order finite volume solver for convection process

In the Strang splitting method, the convection process of the conserved quantities is governed by Euler equation (2.8), for which there are many mature solvers in the market. In this paper, we follow [15] to use a Godunov type finite volume method for (2.8). Please refer to [15] for the detail of the numerical discretization. We briefly summarize the method here, with related numerical issues.

There are three steps in the framework of a Godunov finite volume method, i.e., reconstruction, evolvement, and reaveraging. Three key components in the algorithm are a stable and efficient temporal discretization, a quality solution reconstruction method, and a reliable and efficient Riemann solver.

To match the numerical accuracy of the Strang splitting method, $\mathcal{O}(\Delta t^2)$, we use the TVD second order Runge-Kutta method for the temporal discretization of the Euler equations. To guarantee the stability of the simulation, the size of the time step Δt is chosen by

$$\Delta t = \alpha \frac{\Delta h}{\|\boldsymbol{V}\| + c},$$

where c is the local speed of the sound, and Δh is the size of the current mesh, which is the size of the smallest cell in the mesh.

Solution reconstruction is an important step on delivering high order numerical method. In this paper, following [15], we use non-oscillatory 1-exact reconstruction in each governing cell to obtain a linear variation of the conserved quantity. On a given mesh of the computational domain $\mathcal{T}$, the non-oscillatory 1-exact reconstruction for a governing cell $\mathcal{K} \in \mathcal{T}$ can be briefly summarized as follows. First of all, several reaction

stencils of $\mathcal{K}$ are generated from $\mathcal{K}$ itself, its Neumann neighbors. Then on each reconstruction stencil, a candidate gradient of the reconstructed quantity is obtained based on the cell average and barycenter of each governing cell from the reconstruction stencil. Finally, a convex linear combination of all candidates is used as the final linear variation of the reconstructed quantity in the governing cell $\mathcal{K}$. For the detail of the non-oscillatory k-exact reconstruction, we refer to [15–17] and references therein.

When the left and right states of the conserved quantity on a quadrature point are obtained, it is a Riemann solver who gives an approximation of the flux in the Euler equations. There are many quality choices for the Riemann solver, we refer to [31] for a comprehensive review. In this paper, we follow [31] to use HLLC flux as the numerical flux.

In propagation of the system from t_n to t_{n+1}, the simulation of convection process will take a considerably large part of the whole CPU time. Hence, the improvement of the efficiency on solving Euler equations will significantly improve the efficiency of the proposed algorithm for reactive Euler equations, and we resort to the OpenMP parallelization for the purpose. It is noted that the application of OpenMP on solver is trivial since there is no data race at all in all important components of the algorithm such as the solution reconstruction, calculation of the HLLC flux, and the update of the cell averages. The numerical results in the last section effectively show the acceleration of the simulation with the help of OpenMP.

2.5 *h*-adaptive on simulations

Quality results from the detonation simulations are demanding on the computational resources, because of the requirement on the sufficiently long simulation time, and the restriction on the size of the time steps. Hence, the efficiency is a crucial issue on the practical simulations. In this paper, we mainly adopt *h*-adaptive methods to partially resolve the efficiency issue.

The strategy we used in this paper for the acceleration of the simulations is the *h*-adaptive method. The idea of the adaptive mesh methods is local refinement of the mesh grids when needed, while keep the mesh grids coarse elsewhere. In [15], an *h*-adaptive method has been introduced in the detonation simulations. Briefly, the *Hierarchy Geometry Tree* (HGT) is used to efficiently handle the refinement and coarsening of the mesh grids, the numerical tests in [15] show the effectiveness of the above *h*-adaptive method.

By using HGT, there are two more steps for implementation of h-adaptive methods, i.e., the generation of the error indicator for each element, and the update of the solution from the old mesh to the new mesh.

2.5.1 Error indicator

In [15], a skew Gaussian distribution depending on the location of the detonation front is used to generate the indicator for the adaptive refinement of the mesh girds. However, it depends on the knowledge of the position of the detonation front, and there is no

flexibility for such adaptivity to resolve the fine structure of the reaction in the reaction zone.

In this paper, instead of using skew Gaussian distribution, we design a heuristic error indicator with the two quantities, i.e., the gradient of the pressure and the reaction rate. The error indicator in an element $\mathcal{K}$ at the time t_n is written by

$$Ind_{\mathcal{K}}^n = \left(\int_{\mathcal{K}} (|\nabla p^n|^2 + (w^n)^2) dx \right)^{1/2}. \tag{2.11}$$

The reason of using the two quantities is obvious. The gradient of the pressure will effectively mark the region of the detonation front, while the fine structure of the solution in the reaction zone can be well resolved with the help of the contribution from the reaction rate in the error indicator. To describe the mesh adaptivity process for the propagation of the solutions between two adjacent time instants, we use U_n, U_{n+1} to denote the solutions on the time t_n and t_{n+1}, respectively, and use $\mathcal{T}_n$ and $\mathcal{T}_{n+1}$ to denote the corresponding meshes. First of all, with a given Δt, the solutions propagate on the mesh $\mathcal{T}_n$ from t_n to t_{n+1} by using the Strang splitting method described in last section. Let us use $\tilde{U}_{n+1}$ to denote the corresponding solutions at the time t_{n+1}. Then the following quantity will be calculated in each element.

$$Ind_{\mathcal{K}} = \int_{\mathcal{K}} (|\nabla \tilde{p}^{n+1} - \nabla p^n|^2 + (\tilde{w}^{n+1} - w^n)^2 dx)^{1/2}. \tag{2.12}$$

It is easy to see that the above quantity indicates the variation of the gradient of the pressure, and the reaction rate between two time instants. In our simulations, if the quantity $\sum_{\mathcal{K}} Ind_{\mathcal{K}}$ is greater than a given tolerance, it means that the variation of the two quantities is too large during the time propagation. In this case, we will give up the solution $\tilde{U}^{n+1}$, and repropagate the solution U^n with a reduced time step $\Delta t/2$. This process will be repeated till the tolerance is satisfied. Then, the distribution of the error indicator of the solution $\tilde{U}^{n+1}$ from (2.11) will be calculated, and the mesh $\mathcal{T}_n$ will be locally refined to get the mesh $\tilde{\mathcal{T}}_{n+1}$. It is noted that only mesh refinement is implemented here. Then a conserved interpolation introduced in [15] is implemented for the solution U_n, and we get the updated solution $\tilde{U}_n$ on the mesh $\tilde{\mathcal{T}}_{n+1}$. Finally, the Strang splitting method will be implemented again, and the solution U_{n+1} on the $\mathcal{T}_{n+1} = \tilde{\mathcal{T}}_{n+1}$ is obtained. In the practical implementation, after 4 to 5 propagation steps, the distribution of the error indicators of the solution U_{n+1} on the $\tilde{\mathcal{T}}_{n+1}$ will be calculated, and the mesh will be locally refined and/or coarsened to get $\mathcal{T}_{n+1}$, and the updated U_{n+1}.

With the above adaptivity process, the detonation front as well as the reaction zone can always be resolved well during the dynamics.

2.5.2 Solution interpolation

For the solution updated from the old mesh to the new mesh, we need to take care of two things, i.e., conservation of the cell average and the high resolution of the numerical

solution. With the HGT data structure, this process could be realized easily. Let $\mathcal{T}_o$ and $\mathcal{T}_n$ denote the old mesh and new mesh, respectively. From the property of the HGT data structure, there are following three relations between each two elements from two meshes, i.e., for $\mathcal{K}_o \in \mathcal{T}_o$ and $\mathcal{K}_n \in \mathcal{T}_n$, we have the following relations,

$$\mathcal{K}_o \prec \mathcal{K}_n, \quad \mathcal{K}_o \succ \mathcal{K}_n, \quad \mathcal{K}_o = \mathcal{K}_n.$$

Here $\mathcal{K}_o \prec \mathcal{K}_n$ means $\mathcal{K}_o$ is a child of the element $\mathcal{K}_n$, and $\mathcal{K}_o \succ \mathcal{K}_n$ means $\mathcal{K}_o$ is the parent element of $\mathcal{K}_n$, and $\mathcal{K}_o = \mathcal{K}_n$ means that two elements is the same node in the HGT. Suppose that the relation between two elements K_o and K_n is known, the solution updated from $\mathcal{K}_o$ to $\mathcal{K}_n$ will be implemented as follows in this paper:

- $\mathcal{K}_o \prec \mathcal{K}_n$: $\overline{\boldsymbol{U}}_n += \overline{\boldsymbol{U}}_o * |\mathcal{K}_o| / |\mathcal{K}_n|$;
- $\mathcal{K}_o \succ \mathcal{K}_n$: $\overline{\boldsymbol{U}}_n = \boldsymbol{U}_o(\overrightarrow{X}_{\mathcal{K}_n})$;
- $\mathcal{K}_o = \mathcal{K}_n$: $\overline{\boldsymbol{U}}_n = \overline{\boldsymbol{U}}_o$,

where $|K|$ means the area of the element K, and $\overrightarrow{X}_{\mathcal{K}}$ means the barycenter of the element K. U_o means the reconstructed solution. After updating all solution, we have to rebuild the auxiliary information like reconstruction patches and least-square matrices.

3 Boundary condition and reliable period

Briefly, the scene We are interested in is the free propagation of the detonation wave along an infinitely long channel. In the simulations, with the assumption that the detonation propagates with a constant velocity, we actually attach a moving frame on the detonation front, and impose the appropriate boundary conditions on the inflow and outflow boundaries. It is noted that since the instability of the detonation phenomenon, the dynamics of the detonation front is complicated. However, the mean velocity of the detonation front still agrees with the constant velocity well. Hence, the moving frame configuration works very well generally.

In two-dimensional cases, the computational domain is a rectangle, in which the upper and lower boundaries are the solid walls, and the right and left boundaries belong to the inflow and outflow boundaries, respectively, according to the discussion in above sections. Since the governing equations describe the in-viscid reaction flows, the slip wall boundary conditions can be trivially imposed on the upper and lower boundaries. For the inflow boundary on the right edge of the domain, since the detonation phenomenon studied in this paper are all strong detonations, the supersonic inflow boundary conditions are used, and the flow status outside the domain will be the same to the unburnt status of the reactant.

The nontrivial issue is the boundary condition imposed on the left edge of the computational domain. Since they are strong detonation phenomenon, the subsonic outflow

boundary conditions are needed. This means that all quantities on the left side of the outflow boundary can be determined by the ones from inside of the domain, except for the pressure. Hence, if the pressure is not given accurately on the left side of the outflow boundary, the numerical error would propagate towards the detonation front, and the dynamics of the detonation front would be affected after a sufficiently long time. For a stable detonation case, the perturbation introduced from the inappropriate boundary conditions would only slightly and quantitatively affect the dynamics of the detonation front. However, for the unstable detonation phenomenon, the dynamics of the detonation front would be affected qualitatively, which makes the simulations unreliable.

Unfortunately, since the unpredictability of the dynamics of the product flow around the outflow boundary, there is no general method to give the accurate pressure. The extrapolation technique is popular on handling this issue. It can be seen clearly from the following numerical results that the unstable detonation simulations would be affected qualitatively.

With the parameters $Ea=50.0$, $Q=50.0$, $\gamma=1.2$, two specific cases with different overdriven factors, i.e., $f=1.5$ and $f=1.6$, were studied in detail for the time interval of the reliable observation in [19]. The inequality

$$L \geq CT$$

was given in the paper where T was the desired maximum time for the observation, and L was the corresponding minimum length of the computational domain, and C was a coefficient depending on the detonation velocity and the quantity $u+c$ where c is the sound speed. Although the numerical experiments in [19] confirmed this estimation well, the drawback is also obvious. For example, for the case when $f=1.6$, the inequality was given as $L \geq 1.88T$, with the parameter $C=1.88$. This result was also adopted in [22]. It is noted that in the calculation of the parameter C, the quantity $|u|+c$ is used to estimate the velocity of the error propagation. Hence, the parameter C is actually over estimated. We repeat the simulation from [19] in a longer region $[0,300]$, and the results are shown in Fig. 1. It can be observed that regular fluctuation is destroyed starting from around $t=200$, which means that $L \geq 1.5T$ is needed for the reliable results on the detonation front. This is obviously sharper than that in [19].

The drawback of the over estimation is that the domain size, hence the total amount of the mesh grids will increase, and the simulation efficiency will be slowed down, especially for the high dimensional simulations. In this paper, the above issue is overcame by the following strategy. First of all, with the given configuration of the problem, the ZND solutions of the detonation are derived by the procedure introduced in Appendix 5. Then the solution is used as the initial condition to solve the one-dimensional reactive Euler equations. With a priori knowledge on the stability of the detonation from, for example, the linear stability analysis, the inconsistent behavior of the numerical solution on the detonation front can be observed at some time instant. It is this time which suggests the time interval for the reliable observations, and the parameter C in the relation $L \geq CT$ can be obtained accordingly, and this results can be used in the high dimensional simulations

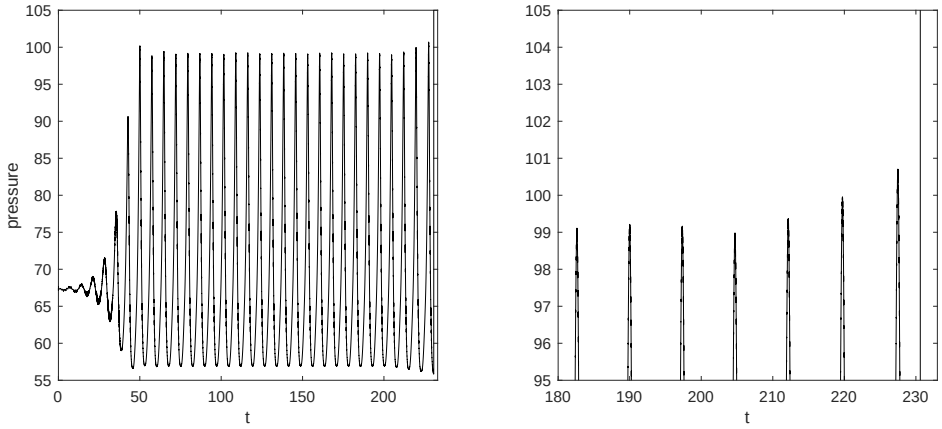

Figure 1: Nonphysical increment of the maximum pressure can be observed after $t=200$.

with the same initial conditions. Since the estimation on the parameter C is done in the one-dimensional case, the extra computational load can be ignored, compared with the one in the high dimensional case.

4 Numerical tests

In this section, we will show some numerical results about the reliable period and h-adaptive simulations. In the following, a variable with subscript u denotes its unburnt status, while the subscript b for its complete burnt status. For example, ρ_u denotes the density of the unburnt gas at the downstream side of the tube ($x=+\infty$), while ρ_b denotes the density of the completely burnt gas at the upstream side of the tube ($x=-\infty$). The initial value is derived from ZND detonation theory which is introduced in Appendix. It is noted that a library is provided for the generation of the ZND results, people may download it from [8].

Physically, the preexponential parameter A in (2.5) represents the frequency of collisions in the correct orientation. Mathematically, this parameter gives us a chance to unify the *half-reaction length* $L^{1/2}$, which is a characteristic length for the simulations of detonation. It is derived from ODE (A.7) that

$$L^{1/2}=\int_{\frac{1}{2}}^{1}-\frac{m}{w}dY. \tag{4.1}$$

To unify $L^{1/2}$, the preexponential factor A needs to be chosen as

$$A=-m\int_{\frac{1}{2}}^{1}1\Big/\left(e^{-\frac{Ea}{T}}\rho Y\right)dY. \tag{4.2}$$

4.1 One-dimensional ZND solutions verification for the observation period

Example 4.1. With the initial state $\rho_u = 1.0$, $P_u = 1.0$, $u_u = 0.0$, the parameters $E_a = 50.0$, $Q = 50.0$, $f = 1.8$, $\gamma = 1.2$, and initial preexponential parameter $A = 200.0$, the profiles of the solutions are given in Fig. 2.

First of all, we use the parameters in Example 4.1 to setup the reactive Euler equations (2.1). In Example 4.1, the preexponential factor $A = 200$ is used first. Then the formula (4.2) gives $A \approx 145.69$ which unifies the half-reaction length $L^{1/2}$.

In the numerical results, two observations can be made. The first one is the numerical convergence. It is noted that the pressure on the Neumann point is around 75.78 with the configuration given in Example 4.1, while the corresponding results of four simulations can be read from Fig. 3. Since $L^{1/2}$ has been unified, there are 20, 40, 80, 160 mesh grids in $L^{1/2}$ in four simulations, respectively. It can be seen obviously that with the refinement of the mesh grids, the amplitude of oscillation will become smaller and the absolute distance between the pressure on the detonation front and the reference value get closer.

The second observation is the nonphysical oscillation appeared with the time evolution. This can be explained by the extrapolation boundary condition used in the simulation at the outflow boundary. Since it is subsonic flow through the outflow boundary, the interior pressure on the domain boundary should be determined by the exterior one, which is unfortunately unavailable. So the extrapolation technique is used in our simula-

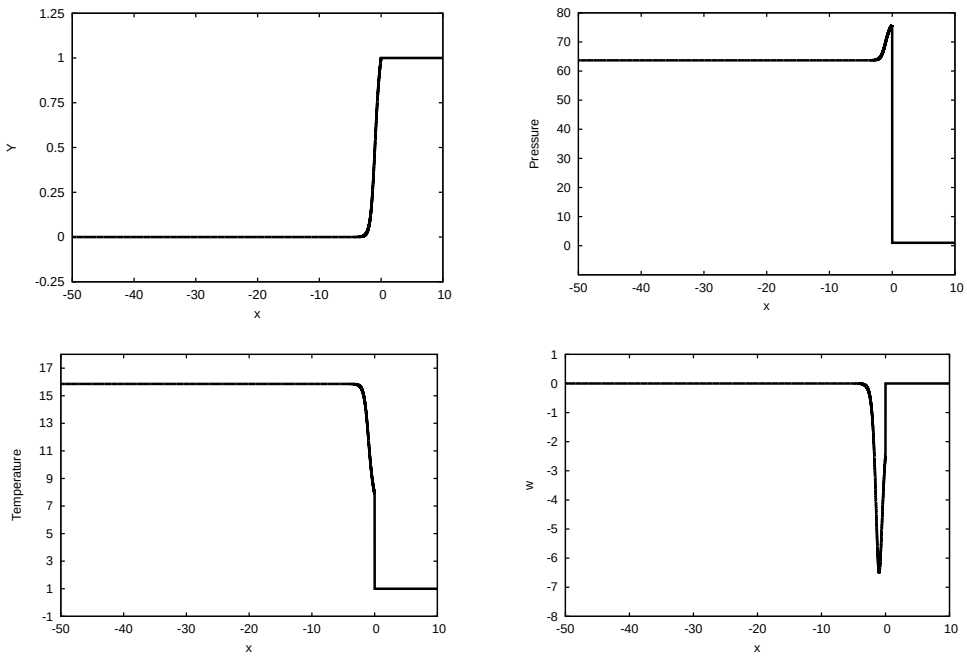

Figure 2: The profiles of mass fraction Y (top left), pressure (top right), temperature (bottom left), and reaction rate w (bottom right) from Example 4.1.

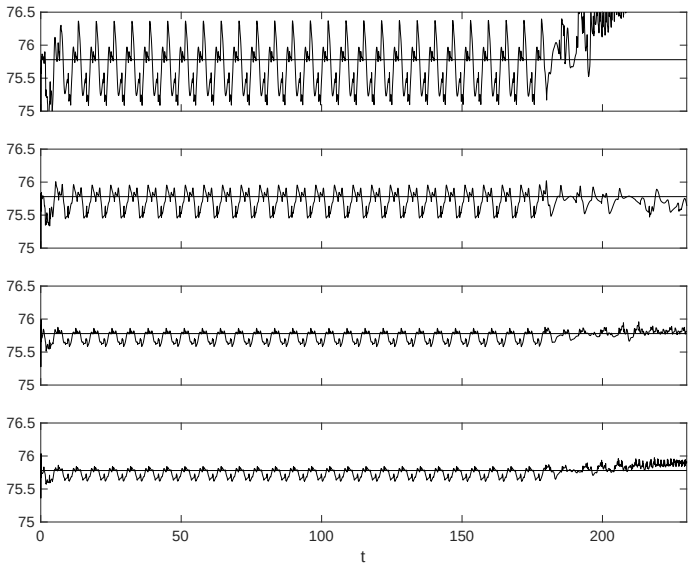

Figure 3: Maximum pressure curves obtained from simulations with the configuration given by Example 4.1. The numbers of grid points in $L^{1/2}$ are, from top to bottom, 20, 40, 80, 160 with $L=300$, respectively. The reliable period is 182 in this case

tions to setup the outflow boundary condition. This improper treatment introduced the numerical error, which finally caused the nonphysical oscillation.

A more interesting observation is that the in the simulation with domain $[0,300]$, the nonphysical oscillation appears around $t=182$, while it is $t=245$ for the domain $[0,400]$, and $t=320$ for the domain $[0,500]$. It is noted that the positions of the leading shock are 280, 380, and 480, respectively. This indicates the relation

$$L>1.62T,$$

which means that to generate a reliable solution at the time T, the length of the computational domain should be at least $1.62T$.

As a comparison, according to [19], there are theoretical analysis about the relation between time and length of domain. The $|u|+c$ wave associated with the first point presumably containing data that have not been updated and thus are corrupted, eventually intercepts the shock. For $f=1.8$ this interception occurs at time

$$T=\frac{L}{u+c-s}+\frac{L}{s}=\frac{L}{2.9}+\frac{L}{9.136},$$

where s is the speed of detonation front. In the end, the theoretical analysis gives a much looser estimation than the numerical results, i.e.,

$$L>2.201T,$$

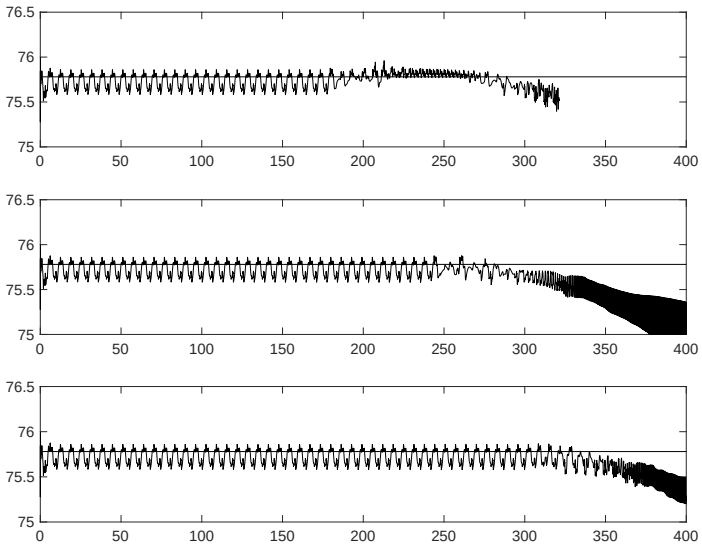

Figure 4: Maximum pressure curves obtained from simulations with the configuration given by Example 4.1. The numbers of grid points in $L^{1/2}$ are, from top to bottom, 80, 400, 500 with $L=300$, respectively. The reliable periods are 182, 245, 320, respectively, in this case.

which indicates that a longer region is needed, to ensure that no corrupted $|u|+c$ waves will be able to catch up with the shock within the computational time of interest. From this comparison, it is noted that considerable computational resources can be saved with the help of the proposed numerical approach, by using a shorter domain.

4.2 One-dimensional four-mode oscillation

Example 4.2. With the initial state $\rho_u=1.0$, $P_u=1.0$, $u_u=0.0$, the parameters $E_a=27.8$, $Q=50.0$, $f=1.0$, $\gamma=1.2$, and initial preexponential parameter $A=56.2266$.

With the above configuration, bifurcation to a four-mode oscillation should be observed [21]. In this example, two main factors affecting the formation of the bifurcation structures, i.e., the mesh resolution and the order of the numerical scheme, will be demonstrated clearly by the numerical experiments.

For the above purpose, three simulations are implemented. The first two are implemented with the proposed numerical framework without the solution reconstruction, which means that the piecewise constant approximation is used in the spatial discretization. From Fig. 5 (left and middle subfigures), it can be seen clearly that the importance on the mesh resolution, i.e., the dynamics of the detonation front with different mesh resolutions are qualitatively different, and it is the mesh with high resolution who gives the reliable results.

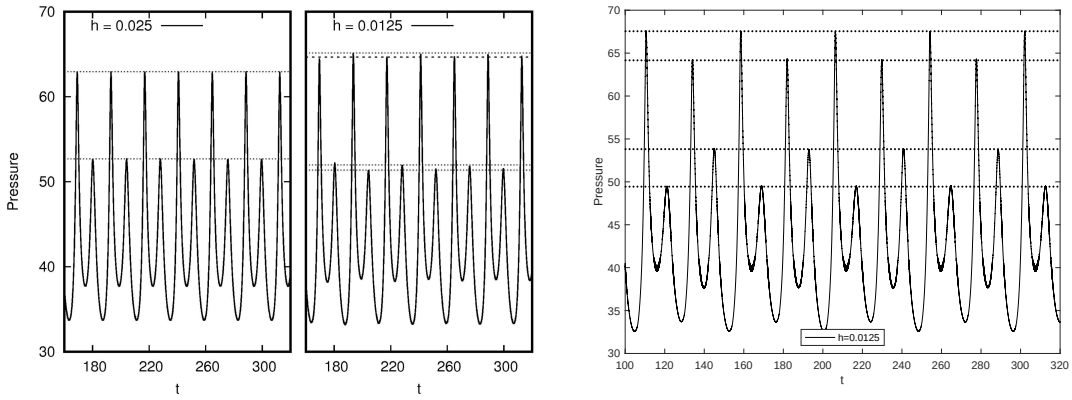

Figure 5: Maximum pressure curves obtained from simulations with the configuration given by Example 4.2 in [21]. The left are results with piecewise constant approximation, and with the numbers of grid points in $L^{1/2}$ 40 and 80, respectively. The right one is the results with piecewise linear approximation, and the number of grid points in $L^{1/2}$ is 80.

The third simulation is devoted to highlighting the importance of the high order numerical methods. In this simulation, the same numerical framework to the previous two simulations is used, except for the using of the non-oscillatory 1-exact solution reconstruction. The advantage of using high order numerical methods is quite obvious, i.e., with 80 grid points in the half reaction zone, the four-mode bifurcation obtained from the simulation agrees with the one from [21] so much better.

4.3 Cell structure simulations

Example 4.3. With the initial state $\rho_u = 1.0$, $P_u = 1.0$, $u_u = 0.0$, the parameters $E_a = 20.0$, $Q = 2.0$, $f = 1.1$, $\gamma = 1.2$, and initial preexponential parameter $A = 1.13437e+06$.

The simulation with the configuration given by Example 4.3 has been studied in several papers, see [3, 10, 15]. In our simulations, the length of the computational domain is chosen as 80.0, and the initial position of the detonation front is 70.0. In these simulation, we will show how to apply the concept about reliable period of observation in numerical simulations.

4.3.1 One-dimensional approximation of reliable period

To estimate a time period of the reliable observation, the numerical experiments in Example 4.1 are reimplemented, with the given parameters in Example 4.3. In Fig. 6, the figure shows the different reliable period in meshes with different domain length. After we zoom in the maximum pressure curve obtained from the mesh size 0.0125, an apparent jump can be observed around $t = 171,249,347,433$ respectfully. Similar to the results showed in Fig. 3, this jump can be explained by the numerical error introduced from the subsonic outflow boundary.

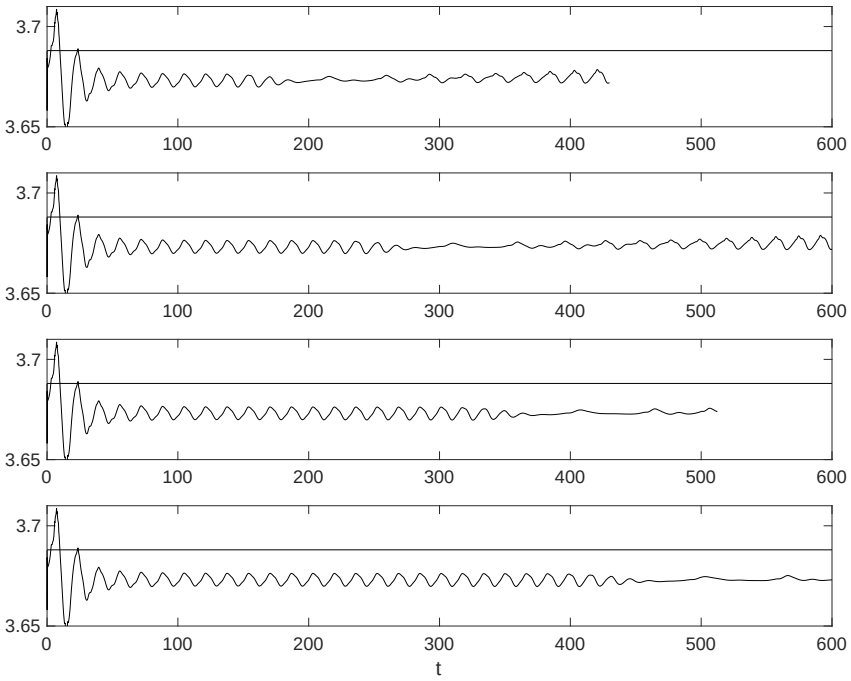

Figure 6: Maximum pressure curves obtained from simulations with the configuration given by Example 4.3. The length of the computational domain are, from top to bottom, 40, 60, 80, 100, respectively, and the number of the mesh grids in $L^{1/2}$ is 80. The reliable periods are 171, 249, 347, 433, respectively, in this case

As a result, in the one-dimensional simulations with the parameters given in Example 4.3, and with the domain length 80.0 and the initial detonation front position 70.0, the time period for the reliable observation of the dynamics of the detonation front is approximately $[0,340]$. In the following simulations, we consider the dynamics of the detonation in a real two-dimensional domain. The domain $[0,10]\times[0,80]$ with $x=70$ as the initial position of the detonation front.

4.3.2 Simulations with two-dimensional uniform refined mesh

In the first simulation, the simulations are implemented on three successively refined meshes. The records of the maximum pressure obtained from first three simulations are showed in Fig. 7 and the pressure distribution for each simulation at $t\approx 200$ are showed in Fig. 8. From Fig. 7, the intrinsic instability of the multi-dimensional detonation is showed obviously, i.e., with the quality right triangle mesh, the periodic pulsation structure eventually appears, no matter how small the mesh size is. More importantly, from all three results, it can be seen that nonphysical oscillation appear around $t=340$, which coincides with the prediction from the one-dimensional results very well. In Fig. 8 the pressure at $t\approx 200$ obtained from three successively refined meshes are showed. At this time, the pe-

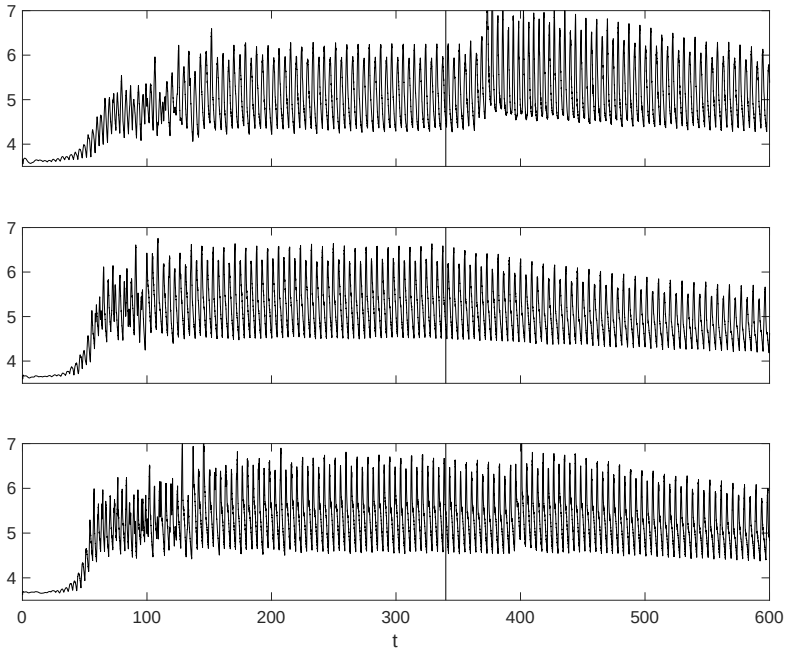

Figure 7: The records of the maximum pressure obtained from simulations on three two-dimensional meshes, which have 25600, 102400, 409600 cells. The vertical line at $t\approx 340$ denotes the reliable period.

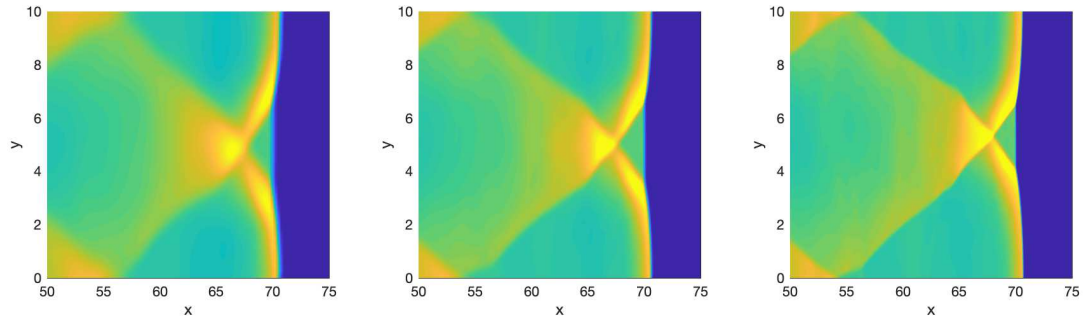

Figure 8: The pressure distributions obtained from simulations on three successively refined meshes, which have 25600, 102400, 409600 cells at $t\approx 200$.

riodic pulsation structure has been formed already, and the numerical convergence can be observed from the results successfully, i.e., with the refinement of the mesh grids, the resolution of the solution becomes higher.

On the other hand, the propagation of the numerical error from the outflow boundary can be observed clearly in Fig. 9, i.e., the motion of a wired line towards the detonation front shows clearly in the figure. When we consider the dynamics of the detonation in Example 4.3 in a real two-dimensional domain, it is well known that cellular structure

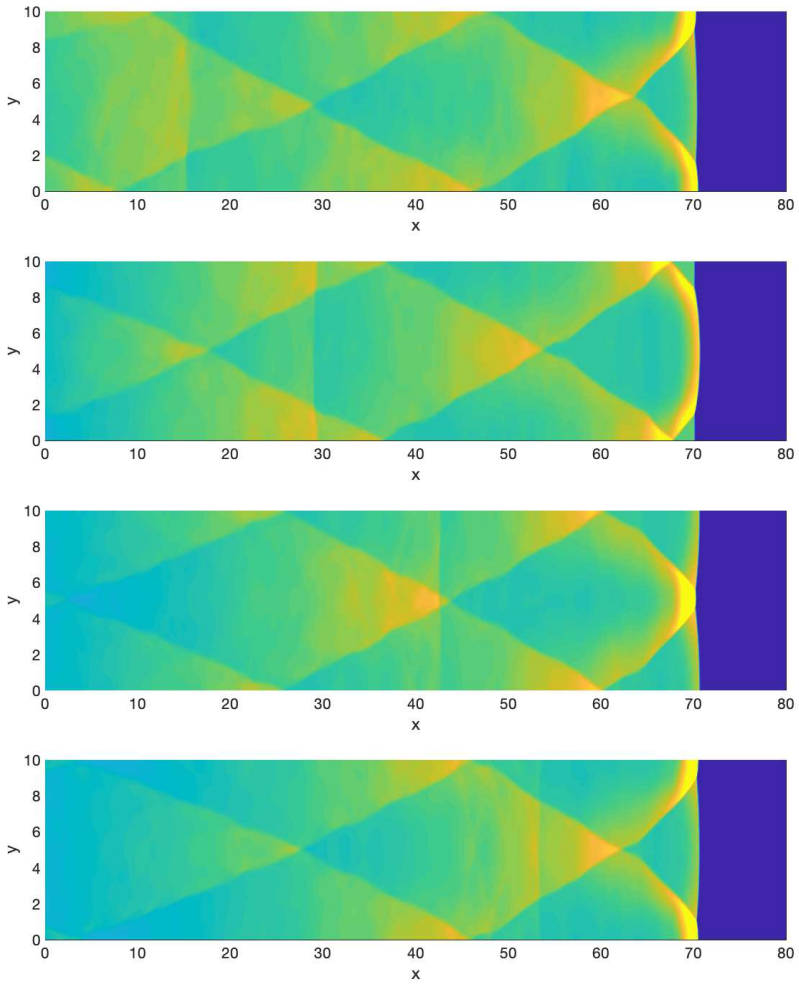

Figure 9: The pressure distributions obtained from simulations on mesh with 409600 cells at $t\approx 200,250,300,340$. There are lines at $x\approx 15,30,42,53$ respectively.

can be observed in the numerical solution, which means that the nontrivial dynamics of the solution appears along the transverse direction on the detonation front. Although the dynamics of the detonation in two-dimensional simulations is quite different from that in the one-dimensional cases, we would like to mention that $[0,340]$ is still a reliable time period for the reliable observation of the detonation dynamics, based on the observation that the estimated velocity of the detonation from ZND theory still works very well in the two-dimensional simulations. Hence, it is reasonable to say that the velocities of the error propagation along the x-axis in both one-dimensional and two-dimensional simulations are approximately equal.

This example shows that to predict a relation between the domain size and the maximum observation time, and then using this relation to guide the high dimensional sim-

ulations, is an effective approach towards the efficient simulations of the reactive Euler equations. In the next example, based on this approach, we introduce the effectiveness of the *h*-adaptive method on further saving computational resources.

4.3.3 Simulations with two-dimensional h-adaptivity

In this subsection, the adaptive module of the proposed method is tested. For the convenience on the comparison, the parameters from the above subsection are still used here.

The results obtained from the simulation are showed in Fig. 10. It can be seen that in the adaptive method, there are 47926 mesh grids in the domain, and the records of the maximum pressure from the adaptive method almost duplicate that from the uniform mesh which has 409600 mesh grids. This is reverified by the pressure in Fig. 10 that they coincide with the ones showed in Fig. 8 very well. In this case, around 90% mesh grids are saved with the help of the adaptive method to reach almost the same accuracy. Fig. 10 shows the distribution of the mesh grids in the whole domain. It can be observed that with the indicators generated by (2.11), most mesh grids are located around the leading shock region and the reaction region, which guarantee the numerical accuracy of the simulations. There are only a small amount of the mesh grids in other regions, which improves the efficiency on the simulation.

Remark 4.1. It can be observed that besides the mesh grids in the reaction zone, the mesh grids in the following region are also refined locally, which forms a long tail in Fig. 10 (top one). This is due to the component with the gradient of the pressure in the error indicator (2.11), which helps effectively on resolving the cell structure caused by the transverse fluctuation on the detonation front.

In the last example, a wider domain $[0,40]\times[0,60]$ is used with the same other configuration. It can be seen from Fig. 11 that multiple cell structures successfully formed

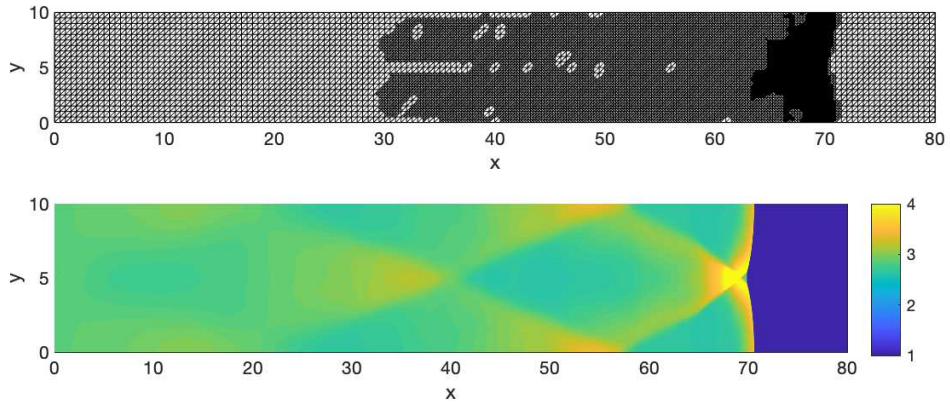

Figure 10: The mesh grids (top), as well as the pressure distribution (bottom), obtained from simulations on adaptive refined meshes(47926 cells) at $t\approx 200$, with the width of the domain 10.

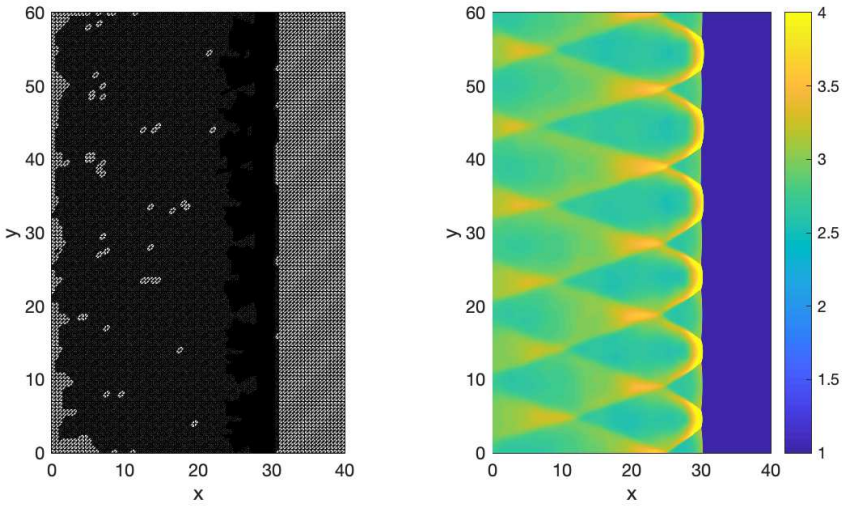

Figure 11: The mesh grids (left), as well as the pressure distribution (right), obtained from simulations on adaptive refined meshes(47926 cells) at $t \approx 70$, with the width of the domain 60.

with 308823 cells. It is worth to mentioning that there are only 2 cells in the half reaction zone for the initial mesh. It is our h-adaptive mesh method which helps effectively on resolving those small structures.

5 Conclusion

In this paper, to study the quality dynamics of the detonation front, an adaptive finite volume method is proposed for the reactive Euler equations. The numerical discretization includes fractional time stepping technique, a second order TVD RungeKutta method for the temporal discretization, and a finite volume method with linear solution reconstruction for the spatial discretization. To restrain the potential numerical oscillation introduced by the high order solution reconstruction, a non-oscillatory k-exact reconstruction is employed. To enhance the efficiency of the algorithm, both the h-adaptive methods and the OpenMP parallelization are introduced in this work.

With the proposed numerical method, two main factors affecting the dynamics of the detonation, i.e., the mesh resolution and the treatment of the subsonic outflow boundary condition, are studied in detail. An effective approach for estimating the relation between the domain size and the maximum observation period in time is proposed, with the help of the quality one-dimensional simulations. Numerical experiments show successfully that the estimation on the maximum observation time instant by our approach is much sharper than the one from the previous theoretical analysis. Numerical results also successfully show the effectiveness of the proposed h-adaptive method on saving the computational resources.

The importance of the high order numerical methods has been demonstrated in our numerical experiments. However, it is nontrivial to raise the order of our current numerical framework since the application of the Strang splitting technique. Furthermore, the application of the viscosity into the model will make the simulations more physical. However, the viscosity will bring solid difficulties on developing quality numerical methods since the existence of the boundary layer, etc. Last but not least, the quality simulation of the propagation of the detonation wave in the complex domain is necessary in the practical applications. We will focus on the above issues in our forthcoming papers.

Acknowledgments

The first author would like to thank the support from the National Natural Science Foundation of China (Grant No. 11771437). The second author would like to thank the support from FDCT of Macao SAR (FDCT 029/2016/A1), MYRG of University of Macau (MYRG2017-00189-FST, MYRG2019-00154-FST), and National Natural Science Foundation of China (Grant Nos. 11922120, 11871489, and 11401608). The third and the fourth authors would like to thank the support from the Science Challenge Project (No. TZ2016002), National Natural Science Foundation of China (Grant No. 11971041). The numerical experiments in this paper are supported by High-performance Computing Platform of Peking University.

Appendix A: ZND detonation theory

In numerical study of detonation phenomenon with reactive Euler equations, numerical solution of one-dimensional ZND model is often used as the initial condition. Below we briefly introduce the ZND model as well as the derivation of the solution.

In ZND model, the detonation process is considered as the convection of the mixture together with the transformation of the mixture from the reactant to the product. Hence, the governing equations consist of the conservation laws and the balance laws. In this paper, for the reaction process, we assume that there are only reactant and product species, and that the reaction is irreversible. Then in one-dimensional case, the reactive Euler equations are given by

$$\frac{\partial}{\partial t}\rho+\frac{\partial}{\partial x}(\rho u)=0, \tag{A.1a}$$

$$\frac{\partial}{\partial t}(\rho u)+\frac{\partial}{\partial x}(\rho u^2+P)=0, \tag{A.1b}$$

$$\frac{\partial}{\partial t}(E)+\frac{\partial}{\partial x}(u(E+P))=0, \tag{A.1c}$$

$$\frac{\partial}{\partial t}(\rho Y)+\frac{\partial}{\partial x}(\rho u Y)=\omega. \tag{A.1d}$$

In the following, we assume that a detonation wave is propagating with a constant velocity s along the x-direction of a tube, and that the flow is steady with respect to a coordinate system moving with the wave. With the given unburnt state of the solutions and parameters, the task now is to determine the velocity s and the burnt state of the solutions, and this can be done by ZND theory as follows.

First of all, a traveling wave coordinate $\xi = x - st$ is introduced, and the above equations (A.1) can be transferred to the following ordinary differential equations

$$-s\frac{d}{d\xi}(\rho)+\frac{d}{d\xi}(\rho u)=0, \tag{A.2a}$$

$$-s\frac{d}{d\xi}(\rho u)+\frac{d}{d\xi}(\rho u^2+P)=0, \tag{A.2b}$$

$$-s\frac{d}{d\xi}(E)+\frac{d}{d\xi}(u(E+P))=0, \tag{A.2c}$$

$$-s\frac{d}{d\xi}(\rho Y)+\frac{d}{d\xi}(\rho u Y)=\omega. \tag{A.2d}$$

By introducing the specific volume $V = 1/\rho$, it can be derived from (A.2a) and (A.2b) the so-called Rayleigh line

$$P(V) = -m^2(V - V_u) + P_u, \tag{A.3}$$

where $m = \rho_u(s - u_u)$ is the mass flux. Then the Hugoniot curve can be derived from (A.2), by using the equation of state, and the quantity enthalpy $h = E - \rho u^2/2 + PV$, as follows

$$P(V,Y) = \left(2Q(1-Y) - P_u V + \frac{\gamma+1}{\gamma-1}P_u V_u\right) \Big/ \left(\frac{\gamma+1}{\gamma-1}V - V_u\right). \tag{A.4}$$

Fig. 12 shows a classical process of a strong ZND detonation. Briefly, the reactant gas is compressed by the leading shock, and the reactant state changes from (V_u, P_u) (solid circle point) to the Neumann point (solid square point) along the Hugoniot curve (dashed one) in Fig. 12. Then the reaction process starts, and the reactant state changes from the Neumann point (solid square point) to the point (V_b, P_b) (solid triangle point) along the upper dashed Rayleigh line. It is noted that the minimum velocity for a detonation wave is the speed of Chapman-Jouguet (CJ) detonation. Similarly, the CJ detonation corresponds to two process showed in Fig. 12, i.e., the leading shock changes the reactant state from the point (V_u, P_u) (solid circle point) to the Neumann point (star point) along the Hugoniot curve (dashed one), then the chemical reaction changes the reactant state from the Neumann point (star point) to the final state (V_b^{CJ}, P_b^{CJ}) (solid diamond point).

Hence, with given ρ_u, u_u, P_u, as well as the parameter γ, Q, and f, the detonation velocity s as well as the mass flux m are obtained as follows. First of all, the mass flux of CJ detonation, m_{CJ}, is defined by

$$m_{CJ}^2 = \gamma\frac{P_u}{V_u} + (\gamma^2-1)\frac{Q}{V_u^2}\left(1+\sqrt{1+\frac{2\gamma P_u V_u}{(\gamma^2-1)Q}}\right). \tag{A.5}$$

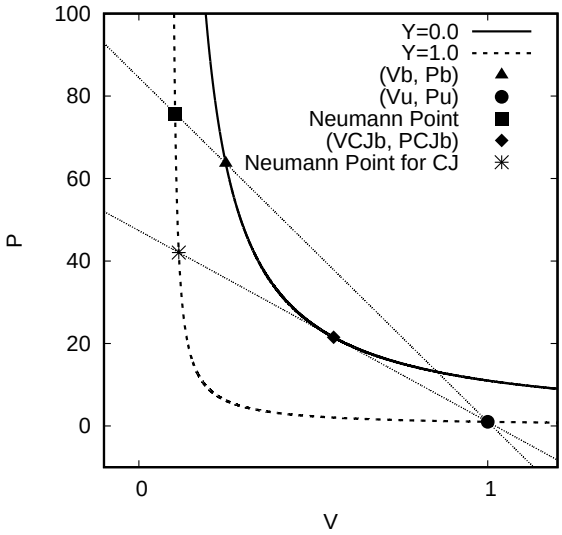

Figure 12: Hugoniot curve and Rayleigh line from ZND theory.

Then the velocity of CJ detonation wave is given by

$$s_{CJ}=\frac{\rho_u u_u+m_{CJ}}{\rho_u}. \tag{A.6}$$

To define a strong detonation, an over-driven factor f is introduced to build the relation between the strong detonation speed s and the CJ detonation speed s_{CJ} as $s^2=fs_{CJ}^2$. From (A.1a), (A.1d), and (A.2a), the following ODE equation can be derived for the distribution of the mass fraction Y in the domain,

$$\begin{cases} \dfrac{d}{d\xi}Y=-\dfrac{\omega}{m}, & \forall\xi<0, \\ Y(0)=1. \end{cases} \tag{A.7}$$

By product rule of the calculus, (A.2d) gives

$$-sY\frac{d\rho}{d\xi}-s\rho\frac{dY}{d\xi}+Y\frac{d\rho u}{d\xi}+\rho u\frac{dY}{d\xi}=w. \tag{A.8}$$

Then replacing the first term on the left side of the above equation by (A.2a), it follows that

$$-Y\frac{d\rho u}{d\xi}-s\rho\frac{dY}{d\xi}+Y\frac{d\rho u}{d\xi}+\rho u\frac{dY}{d\xi}=w. \tag{A.9}$$

After the simplification, we have the following ODE for Y

$$\frac{dY}{d\xi}=\frac{w}{\rho(u-s)}=-\frac{w}{m}, \tag{A.10}$$

with the initial condition $Y(0)=1$.

Finally, with the mass fraction Y, all other quantities are given by

$$P(Y)=\frac{m^2v_u+P_u}{\gamma+1}+\frac{1}{\gamma+1}\beta(Y), \tag{A.11a}$$

$$V(Y)=\frac{\gamma(m^2V_u+P_u)}{m^2(\gamma+1)}-\frac{1}{m^2(\gamma+1)}\beta(Y), \tag{A.11b}$$

$$u(Y)=s-mV(Y), \tag{A.11c}$$

where $\beta(Y)$ is given by

$$\beta(Y)=\sqrt{(m^2V_u-\gamma P_u)^2-2(\gamma^2-1)m^2Q(1-Y)}. \tag{A.12}$$

It is noted that the final state of the solutions can be read from the above functions with $Y=0$.

Remark A.1. A library for the one-dimensional ZND simulations has been released, people may check out the library from the git repository from [8].

References

[1] G. Bao, G. Hu, and D. Liu. An h-adaptive finite element solver for the calculations of the electronic structures. *Journal of Computational Physics*, 231(14):4967–4979, 2012.

[2] W. Bao and S. Jin. The random projection method for stiff detonation capturing. *SIAM Journal on Scientific Computing*, 23(3):1000–1026, 2001.

[3] A. Bourlioux and A. J. Majda. Theoretical and numerical structure for unstable two-dimensional detonations. *Combustion and Flame*, 90(3):211–229, 1992.

[4] G. Cael, H. D. Ng, K. R. Bates, N. Nikiforakis, and M. Short. Numerical simulation of detonation structures using a thermodynamically consistent and fully conservative reactive flow model for multi-component computations. *Proceedings of the Royal Society of London A: Mathematical, Physical and Engineering Sciences*, 465(2107):2135–2153, 2009.

[5] R. Deiterding. *Parallel adaptive simulation of multi-dimensional detonation structures*. PhD thesis, 2003.

[6] W. Döring. On detonation processes in gases. *Annals of Physics*, 43(421-436), 1943.

[7] A. V. Duran and V. Sundararaghavan. Finite element code development for modeling detonation of HMX composites. *AIP Conference Proceedings*, 1793(1):080003, 2017.

[8] F. Yang. ZND Analytical Solution https://github.com/yangfengzzz/CFD_gallery, 2020.

[9] L. Fu, X. Y. Hu, and N. A. Adams. Adaptive anisotropic unstructured mesh generation method based on fluid relaxation analogy. *Communications in Computational Physics*, 10, 2020.

[10] Z. Gao, W. S. Don, and Z. Li. High order weighted essentially non-oscillation schemes for two-dimensional detonation wave simulations. *Journal of Scientific Computing*, 53(1):80–101, Oct 2012.

[11] C. Helzel, R. J. Leveque, and G. Warnecke. A modified fractional step method for the accurate approximation of detonation waves. *SIAM Journal on Scientific Computing*, 22(4):1489–1510, 2000.

[12] A. K. Henrick, T. D. Aslam, and J. M. Powers. Simulations of pulsating one-dimensional detonations with true fifth order accuracy. *Journal of Computational Physics*, 213(1):311–329, 2006.
[13] A. M. Hernández, D. S. Stewart, and B. Lieberthal. An explicit algorithm for imbedding solid boundaries in cartesian grids for the reactive Euler equations. *Combustion Theory and Modelling*, 22(4):714–743, 2018.
[14] T. Y. Hou and P. G. LeFloch. Why nonconservative schemes converge to wrong solutions: error analysis. *Mathematics of Computation*, 62(206):497–530, 1994.
[15] G. Hu. A numerical study of 2D detonation wave with adaptive finite volume methods on unstructured grids. *Journal of Computational Physics*, 331:297–311, 2017.
[16] G. Hu, X. Meng, and N. Yi. Adjoint-based an adaptive finite volume method for 2D steady Euler equations with non-oscillatory *k*-exact reconstruction. *Computers & Fluids*, 139:174–183, 2016.
[17] G. Hu and N. Yi. An adaptive finite volume solver for steady Euler equations with non-oscillatory *k*-exact reconstruction. *Journal of Computational Physics*, 312:235–251, 2016.
[18] X. C. Huang. An adaptive conservative finite volume method for poisson-nernst-planck equations on a moving mesh. *Communications in Computational Physics*, 26:389–412, 2019.
[19] P. Hwang, R. P. Fedkow, B. Merriman, T. D. Aslam, A. R. Karagozian, and S. J. Osher. Numerical resolution of pulsating detonation waves. *Combustion Theory and Modelling*, 4:217–240, 2000.
[20] A. R. Kasimov and D. S. Stewart. On the dynamics of self-sustained one-dimensional detonations: A numerical study in the shock-attached frame. *Physics of Fluids*, 16(10):3566–3578, 2004.
[21] J. H. S. Lee. *The Detonation Phenomenon*. Cambridge University Press, 2008.
[22] Y.S. Lian and K. Xu. A gas-kinetic scheme for multimaterial flows and its application in chemical reactions. *Journal of Computational Physics*, 163:349–375, 2000.
[23] F. K. Lu and E. M. Braun. Rotating detonation wave propulsion: Experimental challenges, modeling, and engine concepts. *Journal of Propulstion and Power*, 30(5):1125–1142, 2014.
[24] S. Macnamara and G. Strang. *Splitting Methods in Communication, Imaging, Science, and Engineering*, chapter Operator Splitting. Springer, 2016.
[25] C. M. Romick and T. D. Aslam. Two-dimensional detonation propagation using shock-fitting. Technical report, Los Alamos National Lab.(LANL), Los Alamos, NM (United States), 2016.
[26] H.-C Salvesen and R. Teigland. Non-reflecting boundary conditions applicable to general purpose CFD simulators. *International Journal for Numerical Methods in Fluids*, 28(3):523–540, 1998.
[27] G.J. Sharpe. Linear stability of idealized detonations. *Proceedings of the Royal Society of London. Series A: Mathematical, Physical and Engineering Sciences*, 453(1967):2603–2625, 1997.
[28] M. Short and D. S. Stewart. Cellular detonation stability. part 1. a normal-mode linear analysis. *Journal of Fluid Mechanics*, 368:229–262, 1998.
[29] N. N. Smirnov, V. F. Nikitin, L. I. Stamov, V. A. Nerchenko, and V. V. Tyrenkova. Numerical simulations of gaseous detonation propagation using different supercomputing architechtures. *International Journal of Computational Methods*, 14(04):1750038, 2017.
[30] T. Tang. Moving mesh methods for computational fluid dynamics. *Contemporary mathematics*, 383:141–174, 2005.
[31] E. F. Toro. *Riemann Solvers and Numerical Methods for Fluid Dynamics: A Practical Introduction*. Springer, 2009.

[32] J. Von Neuman. Theory of detonation waves. Technical report, Institute for Advanced Study Princeton NJ, 1942.
[33] C. Wang, Y. Bi, W. Han, and J. Ning. Large-scale parallel computing for 3D gaseous detonation. *Procedia Engineering*, 61:276–283, 2013. 25th International Conference on Parallel Computational Fluid Dynamics.
[34] C. Wang, X. Dong, and C.-W. Shu. Parallel adaptive mesh refinement method based on WENO finite difference scheme for the simulation of multi-dimensional detonation. *Journal of Computational Physics*, 298:161–175, 2015.
[35] W. Wang, C.-W Shu, H. C. Yee, D. V. Kotov, and B. Sjogreen. High order finite difference methods with subcell resolution for stiff multispecies detonation capturing. *Communications in Computational Physics*, 17:317–336, 2015.
[36] Z. Wang, G. Bao, J. Li, P. Li, and H. Wu. An adaptive finite element method for the diffraction grating problem with transparent boundary condition. *SIAM Journal on Numerical Analysis*, 53(3):1585–1607, 2015.
[37] L. Yang and G. Hu. An adaptive finite element solver for demagnetization field calculation. *Advances in Applied Mathematics and Mechanics*, 11(5):1048–1063, 2019.
[38] Y. B. Zeldovich. On the theory of the propagation of detonation in gaseous systems. *NACA Technical Memorandum*, 1950.
[39] X. Zhang and C.-W Shu. Positivity-preserving high order discontinuous Galerkin schemes for compressible Euler equations with source terms. *Journal of Computational Physics*, 230(4):1238–1248, 2011.
[40] H. Zhu and Z. Gao. An h-adaptive RKDG method with troubled-cell indicator for one-dimensional detonation wave simulations. *Advances in Computational Mathematics*, 42(5):1081–1102, Oct 2016.